Spectrum of *P* and *PcP* in Relation to the Mantle-Core Boundary and Attenuation in the Mantle[1]

HIROO KANAMORI[2]

Seismological Laboratory
California Institute of Technology, Pasadena

Spectrum analyses were made of the records of the short-period vertical component of *P* and *PcP* phases on seismograms of array stations at Tonto Forest, Arizona, for twenty-one earthquakes over the range $\Delta = 47°$ to $83°$. Generally, as has been reported by other investigators, the trace amplitude ratio of *PcP* to *P* is significantly larger than the theoretical ratio. The pulse width of *PcP* is narrower than that of *P*. Both of these facts can be explained by taking into account an appropriate attenuation distribution in the mantle. Taking Q_β, Q for *S* waves, which has been determined by Anderson, Ben-Menahem, and Archambeau using different methods as a standard, the Q distribution for *P* waves, Q_α, can be determined as $Q_\alpha \approx Q_\beta$ at the period of about 1 sec. A matrix method is applied to calculate the complex reflection coefficient of a transitional mantle-core boundary. Impulse responses calculated therefrom and comparison of the waveforms of *P* and *PcP* lead to the conclusion that the major discontinuity at the mantle-core boundary is sharp and is probably less than 1 km thick. The effect of a more gradual transition region superposed upon such a sharp discontinuity is also discussed. The possibility of the existence of a soft layer terminated by a sharp boundary cannot be totally ruled out.

INTRODUCTION

The disagreement between the theoretical and observed amplitude ratio, *PcP/P*, has been discussed by *Martner* [1950], who studied natural earthquakes, and by *Buchbinder* [1965], who studied large explosions. Little attention has so far been paid to the spectral structure of the reflected waves. As has been confirmed by a large number of recent investigations, the mantle is significantly anelastic. The anelasticity will affect the spectral structure of the waves transmitted through the mantle. As *P* and *PcP* take different paths within the mantle, the effects of anelasticity on *P* and *PcP* will be different. Hence it may be possible to extract some information about the attenuative nature of the mantle by comparing the frequency spectrum of *P* with that of *PcP*. Furthermore, since *PcP* is once reflected at the core boundary, the spectral structure of *PcP* should yield some information on the fine structure of the mantle-core boundary. My purpose in this study is to estimate the Q distribution for *P* waves within the mantle and to discuss the nature of the core boundary through the spectrum analysis of *P* and *PcP* phase recorded by short-period Johnson-Matheson seismographs installed at Tonto Forest Seismological Observatory (TFSO), Arizona. The ranges of the periods and the epicenter distances studied here are $T = 0.5$ sec to 2 sec and $\Delta = 47°$ to $83°$, respectively.

DATA

The 16-mm film records from the array stations at TFSO were studied for the interval September 1963 to July 1964. The recording instrument is the Johnson-Matheson short-period vertical seismograph (pendulum period of 1.25 sec, damping factor of 0.54, galvanometer period of 0.33 sec, damping factor of 0.61, and coupling factor of 0.09). The criteria of choosing the records for analysis are (1) both *P* and *PcP* phase are on scale; (2) *P* is impulsive; (3) *PcP* is well separated from other phases, particularly *pP*; and (4) the epicentral distance Δ is large enough so that the difference of the take-off angle at the source of *P* and *PcP* is small.

Criterion (2) is necessary in order to clearly isolate the *P* and *PcP* phase from the back-

[1] Contribution 1412, Division of Geological Sciences, California Institute of Technology.

[2] On leave from Geophysical Institute, Tokyo University.

TABLE 1. List of Earthquakes

Earthquake No.	Date	Origin Time (UT) h m s	Latitude	Longitude	Focal Depth, km	Magnitude (USCGS)	Δ to TFSO, deg	Width of P, sec*	Width of PcP, sec*	Trace Ratio of PcP/P†	Region and Remarks
1	June 23, 1964	02 04 41.8	2.7°S	80.0°W	58	5.2	47.1	0.95	0.75	0.52	Ecuador
2	Dec. 20, 1963	10 48 04.2	5.2°S	80.8°W	55	5.2	48.7	1.1	0.70	0.48	N. coast Peru
3	Oct. 30, 1963	01 17 31.1	4.8°S	77.9°W	20	5.3	50.0	1.5	1.1	0.46	Northern Peru
4	March 22, 1964	07 05 39.7	5.5°S	77.1°W	147	5.1	51.1	0.9	0.8	0.19	Northern Peru
5	June 4, 1964	11 46 01.7	9.6°S	76.1°W	124	5.3	54.9	1.8	1.4	0.33	Central Peru
6	Oct. 7, 1963	12 43 53.6	12.9°S	76.8°W	69	5.4	57.2	1.4	0.7	0.38	Central Peru
7	Nov. 11, 1963	19 54 09.4	9.1°S	71.4°W	585	4.9	57.4	1.2	1.0	0.28	Western Brazil
8	May 28, 1964	12 49 57.5	13.4°S	78.9°W	103	5.2	58.7	1.3	1.0	0.52	Southern Peru
9	July 14, 1964	13 58 28.5	53.3°N	159.7°E	40	5.5	62.7	0.9	0.9	0.48	N. E. coast Kamchatka
10	Oct. 28, 1963	12 03 19.8	52.8°N	159.8°E	33	5.7	62.9	1.4	1.2	0.51	Off E. coast Kamchatka
11	Nov. 6, 1963	18 33 25.9	16.7°S	69.7°W	174	4.7	64.3	0.8	0.7	0.19	Peru-Bolivia border
12	Sept. 20, 1963	22 11 32.2	17.8°S	68.8°W	171	5.1	65.7	1.0	1.0	0.31	Peru-Bolivia border
13	Dec. 29, 1963	17 15 39.2	18.5°S	69.7°W	113	5.5	65.7	1.5	1.1	0.33	Northern Chile
14	July 9, 1964	18 45 32.9	49.4°N	153.5°E	140	5.3	68.0	1.2	1.0	0.25	Sea of Okhotsk
15	Nov. 18, 1963	01 45 27.6	47.2°N	148.5°E	319	4.7	72.0	1.1		0.23	Sea of Okhotsk
16	July 12, 1964	16 48 21.7	24.5°S	66.9°W	164	5.1	72.1	1.0	0.8	0.20	Chile-Argentina border
17	Nov. 17, 1963	13 13 49.3	17.4°S	178.5°W	509	4.7	82.0	0.9		(0.15)‡	Fiji Islands
18	Oct. 27, 1963	08 45 43.8	17.9°S	178.5°W	586	5.0	82.3	1.2		(0.19)	Fiji Islands
19	Dec. 21, 1963	12 34 22.7	21.2°S	175.8°W	90	5.1	82.4	1.4		(0.23)	Tonga Islands
20	Dec. 11, 1963	02 31 19.4	17.8°S	178.6°W	537	4.9	82.4	1.0		(0.13)	Fiji Islands
21	April 26, 1964	14 52 07.6	20.6°S	178.0°W	490	5.1	83.7	1 0		(0.22)	Fiji Islands

* Separation of two minimums or maximums of the main pulse.
† Peak-to-peak amplitude ratio.
‡ Values in parentheses are evaluated by the pulse arriving at time due.

ground noise; (4) is for the purpose of minimizing the effect of radiation pattern at the source, as well as the effect of the crustal layering on the transmission of *P* and *PcP*. The list of earthquakes thus chosen is given in Table 1. Several traces are reproduced in Figure 1. At distances $\Delta = 47°$ to $63°$, *PcP* is generally very clear and *P* and *PcP* are always in phase. *P* and *PcP* in this epicentral range will be discussed later in detail. *PcP* around $\Delta = 70°$ becomes very small, but it is still identifiable, and the direction of the main pulse is the same as that of *P*. At $\Delta \geq 80°$, the reverberation following the initial *P* makes *PcP* identification very difficult. However, the absence of a clear *PcP*, even for comparatively large *P*, implies that the amplitude ratio of *PcP* to *P* becomes extremely small at $\Delta \geq 80°$.

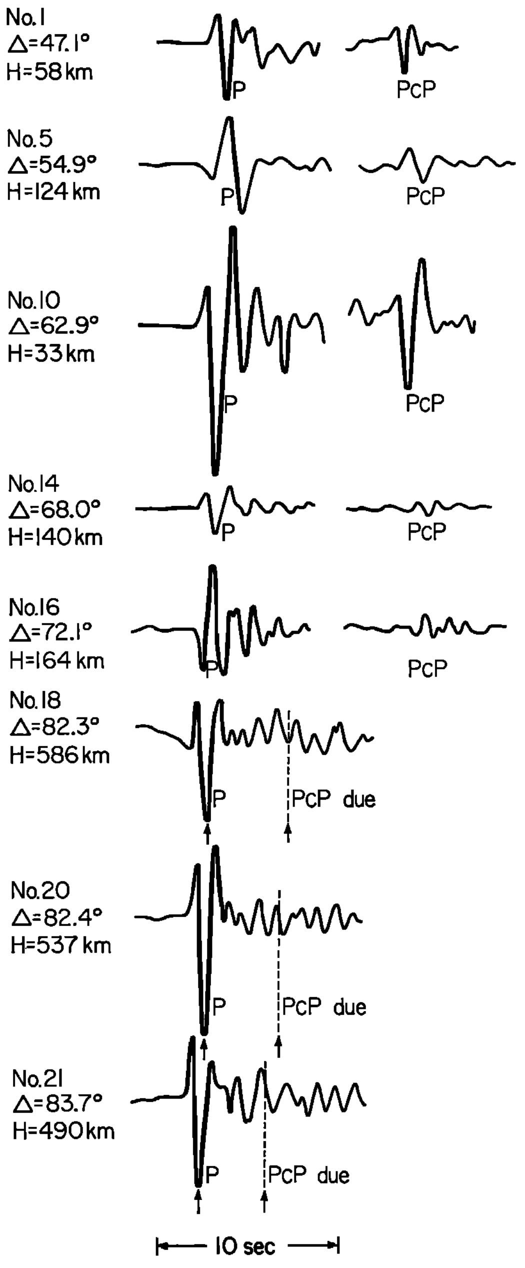

Fig. 1. Vertical component of *P* and *PcP* phases reproduced from TFSO seismograms. Δ is distance and *H* is focal depth.

Interpretation Method

Let us denote the spectrums of *P* and *PcP* at the source by $S(f)$ and $S'(f)$, respectively, as a function of frequency f. The respective frequency spectrums of *P* and *PcP* at the receiver can then be written

$$P(f) = bS(f)G(f)T(f)I(f) \tag{1}$$

$$PcP(f) = b'S'(f)G'(f)T'(f)I(f)rC(f) \tag{2}$$

where b, $T(f)$, and $G(f)$ represent the effect of geometrical spreading, the effect of crustal layering on the transmission, and the effect of attenuation along the path of the *P* wave; b', $T'(f)$, and $G'(f)$ represent the corresponding quantities for *PcP*. $I(f)$, which is common to *P* and *PcP*, is the frequency response of the receiving instrument. $rC(f)$ is the complex reflection coefficient of the mantle-core boundary. Here, r is a real quantity giving the ordinary geometrical reflection coefficient, and $C(f)$ is a complex quantity indicating the transitional nature of the core boundary. $C(f)$ is normalized in such a way that it is unity for infinitely long-period waves; i.e., $C(0) = 1$.

All earthquakes studied here have epicenter distances larger than 47°, so that the difference between the take-off angle of *P* and that of *PcP* at the source is less than about 15°. Under these circumstances, *P* and *PcP* take about the same path within the crust, and also the *PcP* spectrum at the source is considered as approximately the same as the *P* spectrum at the source. Hence we can reasonably assume that

$$S(f) = S'(f) \qquad T(f) = T'(f) \tag{3}$$

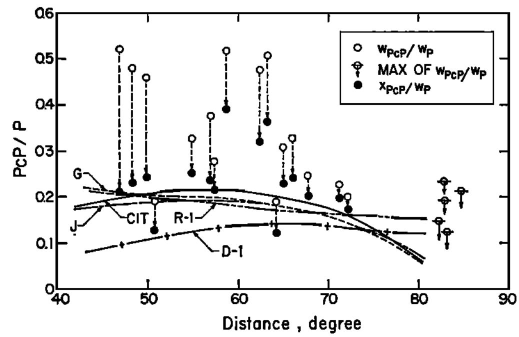

Fig. 2. Amplitude ratio of PcP to P versus epicentral distance. Open circles are determined directly from the seismogram traces and dots are the ratios corrected for the attenuation effect. Curves are $(r\ b' \cos i_{PcP})/(b \cos i_P)$ for Jeffreys (J), Gutenberg (G), CIT 11*A*(CIT), R-1 and D-1 models.

If the specific quality factor for P waves, Q_α, is independent of frequency and is a function only of depth d, $G(f)$ and $G'(f)$ can be written as [*Anderson and Julian*, 1965; *Teng*, 1965; *Carpenter and Flinn*, 1965]

$$G(f) = \exp\left[-\pi f \int_{CP} \frac{ds}{V_P Q_\alpha}\right] \qquad (4)$$

and

$$G'(f) = \exp\left[-\pi f \int_{CPcP} \frac{ds}{V_P Q_\alpha}\right] \qquad (5)$$

where V_p is the P wave velocity as a function of depth d. The integration is taken along the ray path of P in (4) and of PcP in (5). Using (3), (4), and (5), and dividing (1) by (2), we have

$$\frac{P(f)}{PcP(f)} = \frac{b}{rb'} \exp\left[-\pi f H\right] \frac{1}{C(f)} \qquad (6)$$

where

$$H = \int_{CP} \frac{ds}{V_P Q_\alpha} - \int_{CPcP} \frac{ds}{V_P Q_\alpha} \qquad (7)$$

The effect of geometrical spreading, b and b', and the reflection coefficient r at the core boundary can be calculated once a proper elastic earth model is chosen. The data available to us are the time functions of the vertical components of the P and PcP phases which are related to the Fourier transforms of $P(f)$ and $PcP(f)$. The procedure taken here is to compare P and PcP on the basis of several elastic earth models and, by using (6), to determine Q_α and $C(f)$. In the following, three cases are considered.

Analysis

Case 1. Sharp core boundary, no attenuation. As the simplest case, we will first consider nonattenuating earth models which have a sharp mantle-core boundary. Since, in this case, $H = 0$ and $C(f) = 1$, we have from (6)

$$P(f) = (b/rb')PcP(f) \qquad (8)$$

Taking the inverse Fourier transform and considering only the vertical component of the motion, we obtain

$$w_P(t) = \frac{b \cos i_P}{rb' \cos i_{PcP}}\, w_{PcP}(t)$$

where i_P and i_{PcP} are the angles of incidence at the earth's surface of the P and PcP phases. b, b', r, i_P, and i_{PcP} may be more or less dependent on the earth model. In this work, calculations are made for three models: Jeffreys, Gutenberg, and CIT 11. Numerical values for the Jeffreys and Gutenberg models are taken from *Press* [1966], and for CIT 11 model from *Anderson and Toksöz* [1963]. The P wave velocity in the core is taken as 8.1 km/sec for all models, and the ratio of the density of the core to the mantle is taken as 1.7 for the Jeffreys and Gutenberg models and as 1.82 for the CIT 11 model. The method of calculation is similar to the one described by *Dana* [1944, 1945] and, essentially, involves the travel-time calculation.

The comparison of P and PcP is made here only for the amplitude. The open circles in Figure 2 are the observed amplitude ratios of PcP to P for the epicentral distance $\Delta = 47°$ to $83°$. The curves in the figure give the theoretical value $(r\ b' \cos i_{PcP})/(b \cos i_P)$ for the three elastic earth models described above. It is obvious that the observed PcP/P ratio is definitely larger than the theoretical ratio. The observed ratio for $\Delta \geq 80°$ could not be determined well because of the absence of clear PcP phases in the seismograms, but the values over this distance range may be regarded as the maximum possible ratio. As mentioned earlier, the PcP phase can be very clearly identified in seismograms for $\Delta = 47°$ to $63°$.

The discrepancy in this range can hardly be ascribed to observational error. A discrepancy of this sort has already been reported by *Martner* [1950] and *Buchbinder* [1965], but no proper explanation has been given. To account for this discrepancy, we introduce the effect of attenuation in the following.

Case 2. Sharp core boundary, attenuating earth. Figure 3 shows eight pairs of P (top trace) and PcP (middle trace) phases in the range $\Delta = 47°$ to $63°$ reproduced from the seismograms. The first thing we notice is that P and PcP are remarkably alike in shape. This indicates that the phase structures of P and PcP have not been drastically distorted in the course of the transmission. In addition,

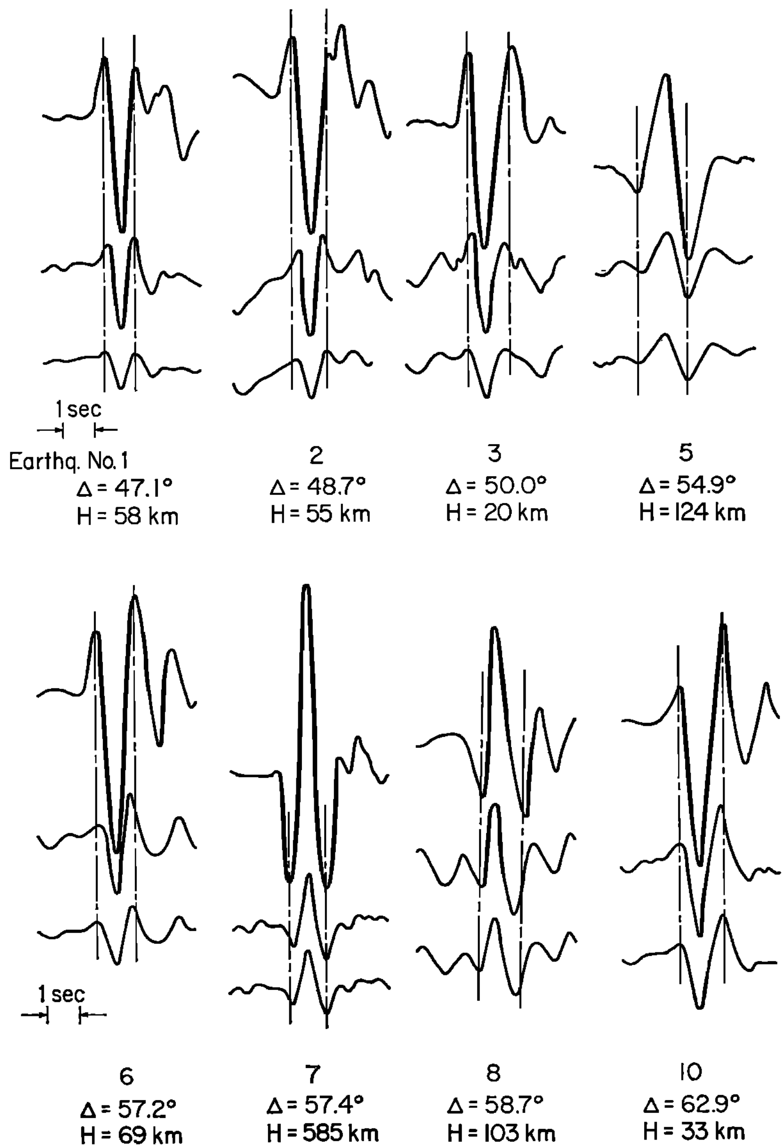

Fig. 3. Eight pairs of P and PcP phase observed over the distance range $\Delta = 47°$ to $63°$. $w_P(t)$ (top trace), $w_{PcP}(t)$ (middle trace), and $x_{PcP}(t)$ (bottom trace) are P, PcP, and PcP corrected for attenuation, respectively. Vertical dashed lines are drawn for the reference of width. H is focal depth.

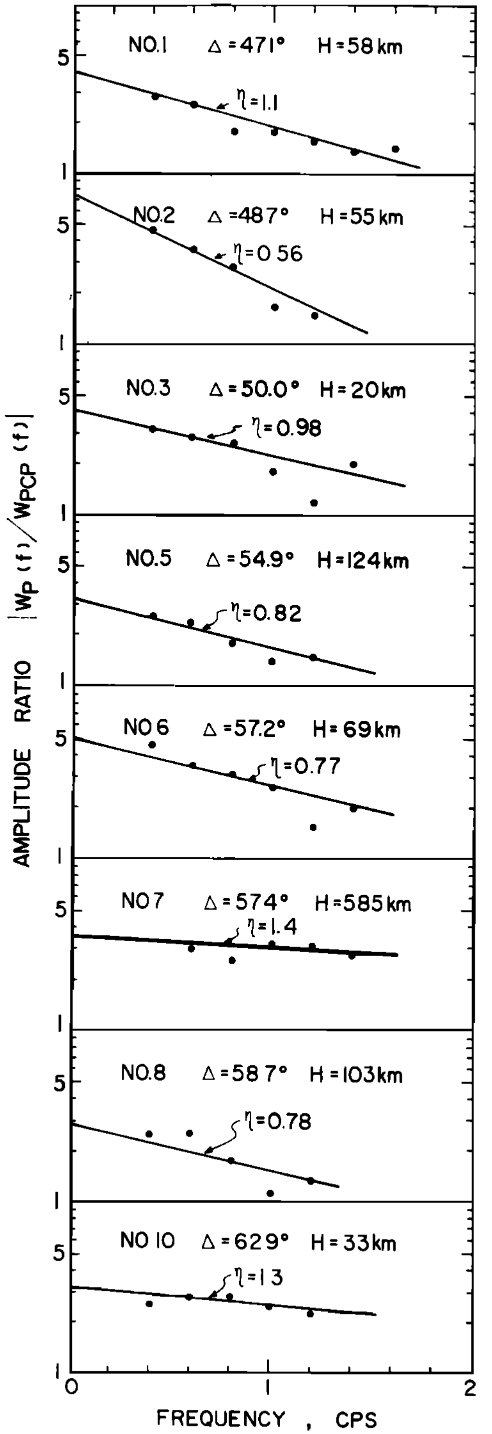

Fig. 4. Ratio of amplitude spectrum of P to PcP versus frequency, for eight earthquakes. Values of η are determined from the slopes of the straight lines.

a more careful inspection reveals that the width of PcP is generally smaller than that of P. This is particularly clear in 1, 2, and 3 of Figure 3. The implication is that, during the transmission, P loses high-frequency components to a greater extent than PcP. This may be expected for a particular Q_α distribution versus depth within the mantle. Since a P wave spends more time in the upper mantle than PcP, it is quite likely that the high-frequency components are highly attenuated in P compared with PcP if the attenuation is higher in the upper mantle than in the lower mantle. The idea that the upper mantle has higher attenuation than the lower mantle has been suggested by *Anderson and Archambeau* [1964] and *Anderson and Kovach* [1964].

A quantitative treatment can readily be made by putting $C(f) = 1$ in (6). Taking the vertical component and logarithm, we can derive from (6)

$$\log \left| \frac{W_P(f)}{W_{PcP}(f)} \right| = -\pi f H \log e + \log \frac{b \cos i_P}{rb' \cos i_{PcP}} \qquad (9)$$

where $W_P(f)$ and $W_{PcP}(f)$ are Fourier transforms of the observed vertical component of P and PcP phase, respectively. $W_P(f)$ and $W_{PcP}(f)$ can be calculated from the seismograms. In our actual calculation a time record of 5 sec duration centered at the main pulse was taken for the analysis. The results are plotted in Figure 4 for eight earthquakes. The general trend that the ratio decreases with increasing frequency reflects the fact that P is more highly attenuated than PcP. Next, it is necessary to specify a Q_α distribution within the mantle. Q_α within the mantle has been studied by *Asada and Takano* [1963], *Anderson et al.* [1965], and *Teng* [1966], but the detailed distribution is not well defined. The following procedure, therefore, is taken for the construction of the Q_α model. Q_β for S waves has been studied by *Press* [1956, 1964], *Fedotov* [1963], *Anderson and Archambeau* [1964], *Anderson and Kovach* [1964], *Anderson et al.* [1965], and *Kovach and Anderson* [1964], using body waves, surface waves, and free-oscillation decay. Now Q_β seems to be known fairly accurately throughout the mantle. In the present study, the Q_β model MM8′, which represents a minor modification of the model given by *Anderson et al.* [1965], is adopted as a standard (Table 2). Although there is no established relation between Q_α and Q_β, it might be a good approximation to assume that

$$Q_\alpha = \eta Q_\beta \tag{10}$$

where η is a constant independent of frequency and depth in the mantle. Thus we have assumed that the shape of the distribution of Q_α throughout the mantle is similar to that of Q_β. The constant η is determined by spectrum analysis of P and PcP (Figure 3). Using (10), we can write (7) as

$$H = \frac{1}{\eta} H_\beta \tag{11}$$

where

$$H_\beta = \int_{C_P} \frac{ds}{V_P Q_\beta} - \int_{C_{PcP}} \frac{ds}{V_P Q_\beta}$$

H_β, which is, of course, a function of Δ and focal depth, can readily be calculated once the Q_β and V_P models throughout the mantle have been specified. The results calculated for models MM8′ and CIT 11 are shown in Figure 5. Although H_β is very small at large Δ, it becomes considerably larger at Δ around 40° to 60°. This is consistent with the trend of the observed discrepancy shown in Figure 2. Substituting (11) into (9) leads to

$$\log \left| \frac{W_P(f)}{W_{PcP}(f)} \right| = -\frac{\pi H_\beta \cdot \log e}{\eta} f + \log \frac{b \cos i_P}{rb' \cos i_{PcP}} \tag{12}$$

with which we can determine the value of η by measuring the slope of the logarithmic plot of amplitude spectrum data (Figure 4). As H_β and ($b \cos i_P / r\, b' \cos i_{PcP}$) are both functions of the epicenter distance and the depth of focus, the plot of $\log | W_P(f)/W_{PcP}(f) |$ for each earthquake should have a different slope and intersection at $f = 0$. By fitting a straight line, we determined the slope independently for each set of $| W_P(f)/W_{PcP}(f) |$. The values of η were then determined from the slopes and are given in Figure 4. The scatter of the values is appreciable. Earthquake 2 gives a particularly small value. This is probably due to the disturbing pulse arriving immediately after the main pulse of P (Figure 3).

If we simply take the mean value and the standard deviation of η, we have $\eta = 0.96 \pm 0.27$. Thus the conclusion is that the MM8′ Q distribution (i.e., $\eta \approx 1$) is a good approximation of Q distribution for P waves of 1 to 2 sec period. The scatter of η may have resulted from the fact that the Q model is not a perfect approximation of the actual distribution. However, in view of the experimental errors, the assumptions made for the frequency independence of Q, and the radiation pattern at the source, the revision of the Q model must await future studies.

TABLE 2. MM8′ Q_β Model

Thickness of Layer H, km	Depth to Bottom of Layer D, km	Q_β
41	41	450
20	61	60
20	81	80
40	121	100
340	461	150
140	601	180
100	701	250
100	801	450
100	901	500
100	1001	600
1897	2898	2300

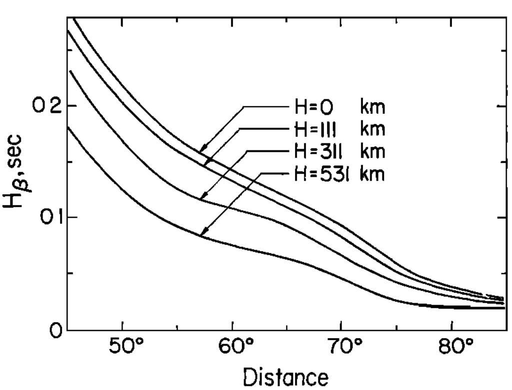

Fig. 5. H_β (differential effect of attenuation on P and PcP) versus distance based on CIT 11A velocity model and MM8′ Q_β model. Curves are given for four focal depths.

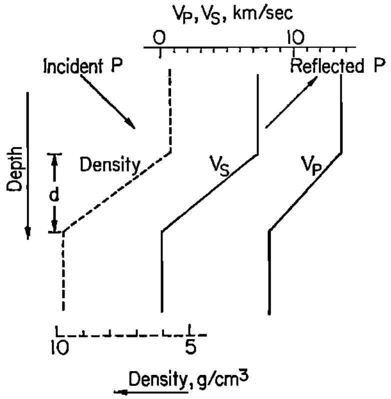

Fig. 6. Transitional solid-to-liquid interface model.

So far, the phase spectrum has been ignored. As the time functions of P and PcP themselves contain phase information, the situation will be made clearer if we go back to the time domain. Taking the vertical component and inverse Fourier transform of (6), we can derive

$$x_{PcP}(t) = \frac{rb' \cos i_{PcP}}{b \cos i_P} w_P(t) \qquad (13)$$

$$x_{PcP}(t) = \int_{-\infty}^{+\infty} w_{PcP}(\tau) a(t - \tau) \, d\tau \qquad (14)$$

where $a(t)$ is the inverse Fourier transform of $\exp[-\pi f H_\beta/\eta]$; that is, when $\eta = 1$,

$$a(t) = \frac{1}{\pi} \frac{2H_\beta}{H_\beta^2 + 4t^2} \qquad (15)$$

Thus, if we convolve the observed PcP with (15), the resulting time function $x_{PcP}(t)$ should have the same shape as the P phase, but the amplitude should be $(r\, b' \cos i_{PcP})/(b \cos i_P)$ times as small as P. The convolution was taken for the eight PcP phases given in Figure 3, and the resulting $x_{PcP}(t)$ are shown at the bottom of Figure 3. The convolution not only reduces the amplitude but also widens the pulse width without distorting the shape. The widths of $x_{PcP}(t)$ and $w_P(t)$ are generally in good agreement. Also, the peak-to-peak amplitude ratios of $x_{PcP}(t)$ to $w_P(t)$, as plotted in Figure 2 by dots, are in closer agreement with the theoretical value than the original ratio $w_{PcP}(t)/w_P(t)$. Thus it can be concluded that the discrepancy of the PcP/P ratio with theory so far reported may satisfactorily be reconciled by taking into account the effect of attenuation within the mantle. The discrepancy still remaining may be due to noise in the observation and also to incorrect assumptions made for the radiation pattern at the source.

Case 3. Transitional core boundary, attenuating mantle. We have shown that the observed spectrum of PcP is satisfactorily explained by an attenuating earth model having a sharp mantle-core boundary. There have been several recent discussions, however, concerning the possible existence of a soft layer near the core boundary [*Dorman et al.,* 1965; *Buchbinder,* 1966; *Sacks,* 1966]. Hence it is worth while to examine the effect of a transitional core boundary on the PcP problem. As discussed by *Dorman et al.* [1965], the present observational travel-time data are not capable of revealing the detailed structure of the mantle-core boundary, and we have to confine ourselves to simple models. Implicit in the transitional boundary might be the idea of iron diffusion into the bottom of the mantle. In this model the density starts increasing in the mantle before the core boundary is reached. This 'diffusion zone' might be terminated by a comparatively sharp change, presumably from solid to liquid. The thickness of this 'solid-to-liquid transition zone' is also of interest. Whether it is of the order of 1 km or 10 km may be difficult to determine by travel-time studies. Although the physical model given here may be oversimplified, it seems reasonable to

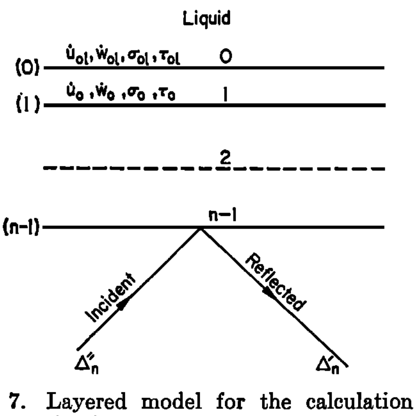

Fig. 7. Layered model for the calculation of complex reflection coefficient. Layer n and 0 correspond to mantle and core, respectively.

consider the effects of the diffusion zone and the solid-to-liquid transition zone separately.

1. Transitional solid-to-liquid interface. As a mathematical model, a transitional solid-to-liquid interface (Figure 6) is considered. The solid layer has elastic constants corresponding to those in the mantle, and the liquid layer has elastic constants corresponding to those in the core. Within the transitional layer of thickness d, P and S wave velocity and density all change linearly with depth. We will assume that the interface and the incident wave front are plane. Since the wavelengths are small compared with the radius of curvature of the core boundary, these assumptions are reasonable, and the Thomson-Haskell matrix method is applicable for the calculation of the complex reflection coefficient of this interface. The general method has been discussed in the works of *Haskell* [1953, 1960, 1962], *Thomson* [1950], and *Wu and Hannon* [1966]. The method is slightly modified here to allow for the liquid layer in place of a vacuum. The transition layer is approximated, as usual, by a laminated structure having $n-1$ layers (Figure 7). (In Figure 7, Haskell's original representation is retained. In applying this layered model to the core boundary, the picture must be inverted.) The Haskell formulation (equation 2.19 in *Haskell* [1953]) relating the displacements and stresses at the surface of the top layer to the amplitude of dilatational and rotational waves in the bottom layer is still valid in this case. That is, using Haskell's notation,

$$(\Delta_n' + \Delta_n'', \Delta_n' - \Delta_n'', \omega_n' - \omega_n'', \omega_n' + \omega_n'') = J(\dot{u}_{0/C}, \dot{w}_{0/C}, \sigma_0, \tau_0)$$

$$J = E_n^{-1} A_{n-1} A_{n-2} \cdots A_1 \qquad (16)$$

Unlike Haskell's case, we cannot put $\sigma_0 = 0$. We let Δ_0' and Δ_0'' be, respectively, the amplitude of descending and ascending dilatational waves in the liquid layer and $\dot{u}_{0l}$, $\dot{w}_{0l}$, σ_{0l}, and τ_{0l} be the velocity components and stress components at the bottom of the liquid layer. We can write, analogously to (2.12) of *Haskell* [1953],

$$\begin{bmatrix} \dot{u}_{0l}/C \\ \dot{w}_{0l}/C \\ \sigma_{0l} \\ \tau_{0l} \end{bmatrix} = \begin{bmatrix} -(\alpha_0/C)^2 & 0 & 0 & 0 \\ 0 & -(\alpha_0/C)^2 r_{\alpha 0} & 0 & 0 \\ \rho_0\alpha_0^2 & 0 & 0 & 0 \\ 0 & 0 & 0 & 0 \end{bmatrix} \begin{bmatrix} \Delta_0' + \Delta_0'' \\ \Delta_0' - \Delta_0'' \\ 0 \\ 0 \end{bmatrix} \qquad (17)$$

where α_0 and ρ_0 are dilatational wave velocity and density, respectively, and $r_{\alpha 0} = [(C/\alpha_0)^2 - 1]^{1/2}$. Boundary conditions here are $\dot{w}_{0l}/C = \dot{w}_0/C$, $\sigma_{0l} = \sigma_0$, and $\tau_0 = \tau_{0l} = 0$. Introducing these boundary conditions and eliminating $\dot{u}_{0l}/C$ and $\dot{u}_0/C$ from (16) and (17), we can determine the reflection coefficient R for the dilatational wave. In case of dilatational input, we put $\omega_n'' = 0$ and $\Delta_0' = 0$ and obtain

$$R = \frac{\Delta_n'}{\Delta_n''} = \frac{(J_{31} - J_{41})[p(J_{22} + J_{12}) + q(J_{13} + J_{23})] + (J_{11} + J_{21})}{(J_{31} - J_{41})[-p(J_{22} - J_{12}) + q(J_{13} - J_{23})] + (J_{11} - J_{21})} \cdot \frac{[p(J_{42} - J_{32}) - q(J_{33} - J_{43})]}{[p(J_{42} - J_{32}) - q(J_{33} - J_{43})]} \qquad (18)$$

where $p = (\alpha_0/C)^2 r_{\alpha 0}$, $q = \rho_0\alpha_0^2$, and J_{ij} are $i\,j$ elements of Haskell's J matrix. R is generally a very complicated complex function and the results can best be shown in the form of an impulse response, the Fourier transform of R. Since the highest frequency involved here is 2 cps, it is reasonable to consider the response for the input

$$\tilde{\delta}(t) = 4 \sin [2\pi(t/0.5)]/[2\pi t/0.5]$$

In Figure 8 the initial part of the response $c(t)$ for the angle of incidence $i_c = 53°$ is shown as an example. When the thickness of the

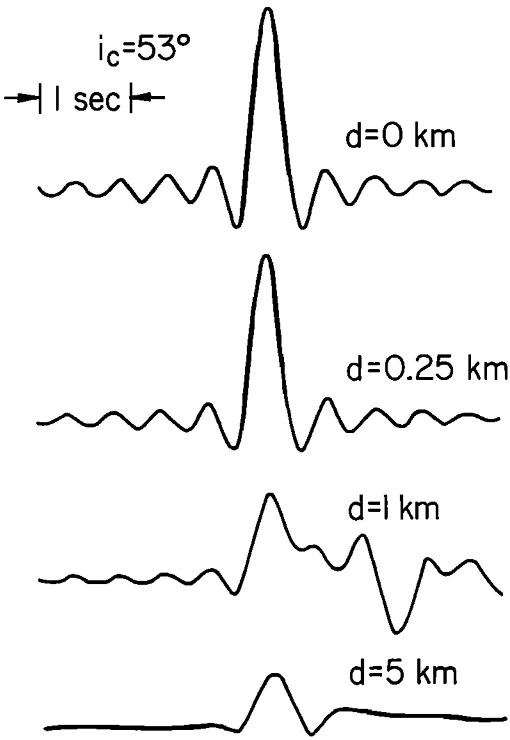

Fig. 8. Initial part of impulse response of P wave reflection at the interface model given in Figure 6. Input is $\bar{\delta}(t) = 4 \sin [2\pi(t/0.5)]/[2\pi t/0.5]$, and the angle of incidence is 53°. Later arrivals are not shown in the figure.

transitional layer is 5 km, the reflection is very small, as expected. When d decreases to about 1 km, the pulse shape becomes quite distorted. This is mainly due to the effect of P to S wave conversion within the transitional layer. This effect disappears, as shown in Figure 8, when the discontinuity becomes still sharper ($d \leq$ 0.25 km). The result, of course, depends on the transitional layer model. The conclusion, however, would still remain qualitatively unchanged. A more specific discussion can be made as follows.

From (6) we can derive

$$x_{PcP}(t) = \frac{rb' \cos i_{PcP}}{b \cos i_P} x_P(t)$$

$$x_P(t) = \int_{-\infty}^{+\infty} w_P(\tau)c(t - \tau)\, d\tau$$

This means that the core response $c(t)$, when convolved with $w_P(t)$, should give the same waveform as $x_{PcP}(t)$ with the amplitude ratio $(r\, b' \cos i_{PcP})/(b \cos i_P)$. As noted earlier, we have already obtained consistent results with $c(t) = \delta(t)$ and $\eta = 1$ (i.e., sharp core boundary and $Q_\alpha = Q_\beta$). As an example, convolutions of $w_P(t)$ and $c(t)$ are calculated for earthquake 1 ($\Delta = 47.1°$) and the results are shown in Figure 9. In this figure are also shown $x_{PcP}(t)$ for $\eta = 1$, 0.5, and 0.2. Comparison of $x_P(t)$ and $x_{PcP}(t)$ clearly indicates that if d is larger than 5 km it would be difficult, whatever value is given to η, to get a consistent width and amplitude ratio. For $d \approx 1$ km the phase structure of $x_P(t)$ is too distorted to be compared with $x_{PcP}(t)$. From these considerations it is quite likely that a very sharp discontinuity, the thickness of which is probably a fraction of a kilometer, exists somewhere within the mantle-core boundary. This does not exclude, however, the possible existence of a superposed transitional layer.

2. Effect of diffusion layer. *Dorman et al.* [1965] have suggested, from studies of free oscillations, the existence of a soft layer at the bottom of the mantle. In their R-1 model this soft layer is 30 km thick. The effect of such a

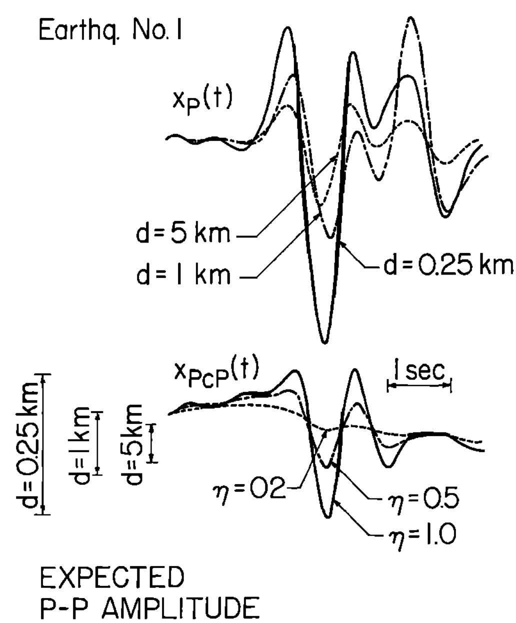

Fig. 9. Comparison of $x_P(t)$ and $x_{PcP}(t)$. Arrows show the expected peak-to-peak amplitudes of $x_{PcP}(t)$ corresponding to $x_P(t)$ for various values of d shown above.

layer on *PcP* will be discussed here. As the wavelengths considered here are about 10 km, ordinary ray theory is applicable for the treatment of the transitional layer extending over a thickness of about 30 km. Two models are considered here (Figure 10). One is the R-1 model proposed by Dorman et al., and the other is the extreme case of diffusion, the D-1 model. This model simulates an extreme diffusion zone in which the fractional iron content increases up to 100% toward the mantle-core boundary. The layer is terminated by a sharp discontinuity due to iron melting. b, b', i_P, i_{PcP}, and r were recalculated for these models. Although the changes in b, b', i_P, and i_{PcP} are very small, r is significantly affected for two reasons. First, the geometrical reflection coefficient at the sharp boundary is different for these models (Figure 11), and, second, as the result of the ray being bent downward because of the low-velocity layer at the bottom of the mantle, the relation between Δ and the angle of incidence i_c at the core boundary is changed as shown in Figure 11. The over-all effect is shown in terms of $(r\ b' \cos i_{PcP})/(b \cos i_P)$ in Figure 2. At $\Delta < 70°$, curve D-1 gives a smaller ratio than the standard models, and the agreement with the observed ratio $[x_{PcP}(t)/w_P(t)]$ becomes appreciably poorer. R-1 gives about the same ratio as the standard

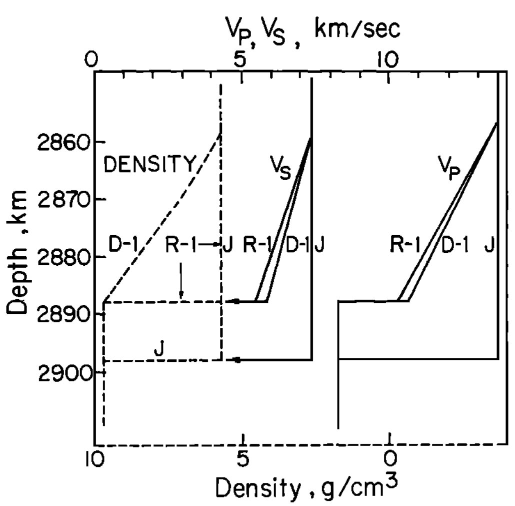

Fig. 10. 'Diffusion zone' models of core boundary. Jeffreys model (J) is shown as reference. Main difference between R-1 and D-1 models is in the density distribution.

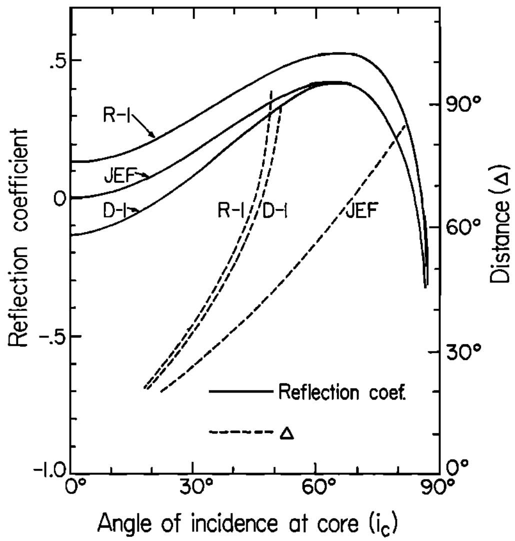

Fig. 11. Reflection coefficient (left ordinate) and epicenter distance (right ordinate) versus angle of incidence at core boundary for Jeffreys (J), R-1, and D-1 models.

models. At $\Delta \geq 80°$, D-1 and R-1 models give higher ratios than the standard models, mainly because of the downward bending of the ray near the core boundary. Unfortunately, the *PcP* phase at $\Delta \geq 80°$ is usually disturbed by other phases on the seismograms, and the amplitude ratio may be uncertain by a factor of 2. It is therefore difficult to say at present which type of core boundary is more consistent with the observed ratio at this range. Although the D-1 model, which simulates the most extreme case of diffusion, is inconsistent with the data at $47° \leq \Delta \leq 70°$, the possibility of the existence of a diffusion layer of less magnitude cannot be totally ruled out.

Discussion

Because the effect of attenuation appears in a more pronounced way for short-period waves than for long-period waves, short-period waves can be used to advantage for the present purpose. Implicit in the present method, however, is the assumption made for the standard distribution of Q_β within the mantle. The result may be changed if the standard model Q_β is modified. As the wavelength studied here is fairly short, about 10 km, scattering due to the inhomogeneities within the earth, particularly in the upper mantle, might contribute to some extent to the apparent attenuation of the waves. *Asada and Takano* [1963] have studied Q_α in the upper mantle by spectrum analysis of short-period P waves. They give a very high Q in the upper mantle, and the present result is inconsistent with their results. Inherent in their discussion is an assumption regarding the source spectrum. The period of the waves studied by them is very short and the source spectrum in the short-period range is totally unknown at present. To account for this discrepancy, therefore, future studies of the short-period source spectrum are necessary. *Teng* [1966] has made extensive studies of P, pP, and S spectrums and has determined the Q_α distribution within the mantle. The present Q distribution is in good agreement with his result, except near the core boundary.

It should be noted that the Q is estimated here at the period of about 1 sec, whereas the MM8′ Q_β distribution was determined by using long-period waves ($T \geq 50$ sec). Since the frequency independence of Q has not been confirmed over the wide frequency range, the present conclusion, $Q_\alpha = Q_\beta$, should not be taken as a general relation between Q_α and Q_β. What is inferred from the present study is that Q_α at $T \approx 1$ sec is about the same as Q_β at long periods. Spectrum analysis is usually strongly disturbed by interfering phases on the seismograms. Consequently, it is vital in the more detailed studies to improve the S/N ratio of the record by developing some signal-enhancing techniques for the PcP phase.

A more detailed determination of the structure of the core boundary will require a much wider frequency range.

Acknowledgments. I am indebted to Dr. Don Anderson for critically reading the manuscript and offering suggestions for its improvement. Thanks are also extended to Dr. Francis Wu for the use of his computer program for the calculation of the complex reflection coefficient. I have benefited from many discussions with Drs. James Brune, Hewitt Dix, Lane Johnson, Stewart Smith, and Ta-Liang Teng.

This research was partially supported by the Advanced Research Projects Agency and was monitored by the Air Force Office of Scientific Research under contract AF-49(638)-1337.

References

Anderson, D. L., and C. B. Archambeau, The anelasticity of the earth, *J. Geophys. Res., 69,* 2071–2084, 1964.

Anderson, D. L., A. Ben-Menahem, and C. B. Archambeau, Attenuation of seismic energy in the upper mantle, *J. Geophys. Res., 70,* 1441–1448, 1965.

Anderson, D. L., and B. R. Julian, Travel times, velocities and amplitudes of body phases (abstract), presented at the annual meeting of Seismological Society of America, St. Louis, April 1965 .

Anderson, D. L., and R. L. Kovach, Attenuation in the mantle and rigidity of the core from multiply reflected core phases, *Proc. Natl. Acad. Sci. U.S., 51,* 168–172, 1964.

Anderson, D. L., and M. N. Toksöz, Surface waves on a spherical earth, 1, Upper mantle structure from Love waves, *J. Geophys. Res., 68,* 3483–3500, 1963.

Asada, T., and K. Takano, Attenuation of short period *P* waves in the mantle, *J. Phys. Earth, 11,* 25–34, 1963.

Buchbinder, G. G. R., *PcP* from the nuclear explosion Bilby, September 13, 1963, *Bull. Seismol. Soc. Am., 55,* 441–461, 1965.

Buchbinder, G. G. R., *PcP* travel times from Longshot and the density ratio of the mantle-core boundary (abstract), *Trans. Am. Geophys. Union, 47*(1), 165, 1966.

Carpenter, E. W., and E. A. Flinn, Attenuation of teleseismic body waves, *Nature, 207,* 745–746, 1965.

Dana, S. W., The partition of energy among seismic waves reflected and refracted at the earth's core, *Bull. Seismol. Soc. Am., 34,* 189–197, 1944.

Dana, S. W., The amplitude of seismic waves reflected and refracted at the earth's core, *Bull. Seismol. Soc. Am., 35,* 27–35, 1945.

Dorman, J., Jerome Ewing, and L. E. Alsop, Oscillations of the earth: New core-mantle boundary model based on low-order free vibrations, *Proc. Natl. Acad. Sci., U. S., 54,* 364–368, 1965.

Fedotov, S. A., The absorption of transverse seismic waves in the upper mantle and energy classification of near earthquakes of intermediate focal depth, *Bull. Acad. Sci. USSR, Geophys. Ser., English Transl.,* no. 6, 509–520, 1963.

Haskell, N. A., The dispersion of surface waves in multilayered media, *Bull. Seismol. Soc. Am., 43,* 17–34, 1953.

Haskell, N. A., Crustal reflection of plane *SH* waves, *J. Geophys. Res., 65,* 4147–4150, 1960.

Haskell, N. A., Crustal reflection of *P* and *SV* waves, *J. Geophys. Res., 67,* 4751–4767, 1962.

Kovach, R. L., and D. L. Anderson, Attenuation of shear waves in the upper and lower mantle, *Bull. Seismol. Soc. Am., 54,* 1855–1864, 1964.

Martner, S. T., Observations on seismic waves reflected at the core boundary of the earth, *Bull. Seismol. Soc. Am., 40,* 95–109, 1950.

Press, F., Rigidity of the earth's core, *Science, 124,* 1204, 1956.

Press, F., Seismic wave attenuation in the crust, *J. Geophys. Res., 69,* 4417–4418, 1964.

Press, F., Seismic velocities, in *Handbook of Physical Constants*, edited by S. P. Clark, Jr., section 9, pp. 195–218, *Geol. Soc. Am. Mem.* *97*, 1966.

Sacks, S., Diffracted wave studies of the earth's core, 1, Amplitudes, core size, and rigidity, *J. Geophys. Res.*, *71*, 1173–1181, 1966.

Teng, T. L., Amplitude of body waves, *Tech. Rept., Contract AF-49(638)-1337*, Seismological Laboratory, California Institute of Technology, Pasadena, 1965.

Teng, T. L., Body-wave and earthquake source studies, chapter 7, Attenuation of body waves and the *Q* structure of the mantle, Thesis, California Institute of Technology, Pasadena, 1966.

Thomson, W. T., Transmission of elastic waves through a stratified solid medium, *J. Appl. Phys.*, *21*, 89–93, 1950.

Wu, F. T., and W. J. Hannon, *PP* and the crustal structure, *Bull. Seismol. Soc. Am.*, in press, 1966.

(Received July 2, 1966;
revised September 22, 1966.)